Baes, M., Sobolev, S. V. (2017): Mantle Flow as a Trigger for Subduction Initiation: A Missing Element of the Wilson Cycle Concept. - *Geochemistry Geophysics Geosystems (G3)*, *18*, 12, pp. 4469—4486.

DOI: http://doi.org/10.1002/2017GC006962

AGU PUBLICATIONS

Geochemistry, Geophysics, Geosystems

RESEARCH ARTICLE
10.1002/2017GC006962

Mantle Flow as a Trigger for Subduction Initiation: A Missing Element of the Wilson Cycle Concept

M. Baes[1] and S.V. Sobolev[1,2]

[1]GFZ German Research Center for Geosciences, Potsdam, Germany, [2]Institute of Earth and Environmental Science, University of Potsdam, Potsdam-Golm, Germany

Key Points:
- Mantle suction flow can act as a trigger for subduction initiation
- Subduction initiation along passive margins is a long-term process, which takes several tens of million years even in 2-D models
- Subduction initiation, induced by mantle suction flow, may occur in future at passive margins along the Argentine Basin and U.S. East Coast

Supporting Information:
- Supporting Information S1
- Table S1

Correspondence to:
M. Baes,
baes@gfz-potsdam.de

Citation:
Baes, M., & Sobolev, S.V. (2017). Mantle flow as a trigger for subduction initiation: A missing element of the Wilson Cycle concept. *Geochemistry, Geophysics, Geosystems*, *18*, 4469–4486. https://doi.org/10.1002/2017GC006962

Received 10 APR 2017
Accepted 16 NOV 2017
Accepted article online 20 NOV 2017
Published online 12 DEC 2017

Abstract The classical Wilson Cycle concept, describing repeated opening and closing of ocean basins, hypothesizes spontaneous conversion of passive continental margins into subduction zones. This process, however, is impeded by the high strength of passive margins, and it has never occurred in Cenozoic times. Here using thermomechanical models, we show that additional forcing, provided by mantle flow, which is induced by neighboring subduction zones and midmantle slab remnants, can convert a passive margin into a subduction zone. Models suggest that this is a long-term process, thus explaining the lack of Cenozoic examples. We speculate that new subduction zones may form in the next few tens of millions of years along the Argentine passive margin and the U.S. East Coast. Mantle suction force can similarly trigger subduction initiation along large oceanic fracture zones. We propose that new subduction zones will preferentially originate where subduction zones were active in the past, thus explaining the remarkable colocation of subduction zones during at least the last 400 Myr.

1. Introduction

In spite of the lack of any Cenozoic examples (Stern, 2004), passive margins are among the first to have been proposed as candidate locations for the nucleation of new subduction zones. The broad acceptance of these tectonic settings arises from the role that they play in the Wilson Cycle (Wilson, 1966), which describes the repeated opening and closing of ocean basins. The collapse of passive margins is essential in the closing phase of the Wilson Cycle; however, the absence of conversion of any passive margins into active ones since the Cenozoic makes the Wilson Cycle a challenging and debatable topic among geoscientists. Among typical present-day examples of old passive margins are the Atlantic margins, where seafloor spreading in the Atlantic Ocean began approximately 185 Ma, following rifting between North America and Africa. The history of rifting and seafloor spreading is well preserved, as there are no active margins around the Atlantic Ocean apart from the Puerto Rico/Lesser Antilles subduction around the eastern Caribbean Sea, and the South Sandwich subduction south of South America. Recently, Duarte et al. (2013), using seismic data, proposed that a new subduction zone is forming along the southwest Iberian margin as a result of propagation of compressive stresses from the Gibraltar Arc, and stresses associated with Africa-Eurasia convergence.

Previous modeling studies have attempted to investigate the possibility of the conversion of Atlantic passive margins into active margins, and the triggering factors involved in this process (Cloetingh et al., 1982, 1984, 1989; Faccenna et al., 1999; Kemp & Stevenson, 1996; Nikolaeva et al., 2010; Regenauer-Lieb et al., 2001); however, to our knowledge, there have not yet been any successful simulations of subduction initiation along a mature passive margin with a realistic continental lithospheric thickness of more than 100 km, and a continental crustal thickness of approximately 35 km. The reason, as was illustrated in the comprehensive modeling study of Nikolaeva et al. (2010, Figure 11), is that due to the high strength of the thick lithosphere, the buoyancy force alone is not sufficient to destabilize the margin, and to break it requires either a crust thicker than 40 km, or additional forcing factors.

Here we introduce and test a new hypothesis for triggering subduction initiation along passive margins: mantle suction force. There is a growing recognition of the important role of the forces implied by mantle flow in various tectonic settings (Becker & Faccenna, 2011; Becker & O'Connell, 2001; Lu et al., 2015), but not yet for passive margins. In Atlantic passive margins, mantle suction flow can be induced either from the long-lived subduction zones of the North and East Pacific Ocean and Nazca Plate, including the Aleutians,

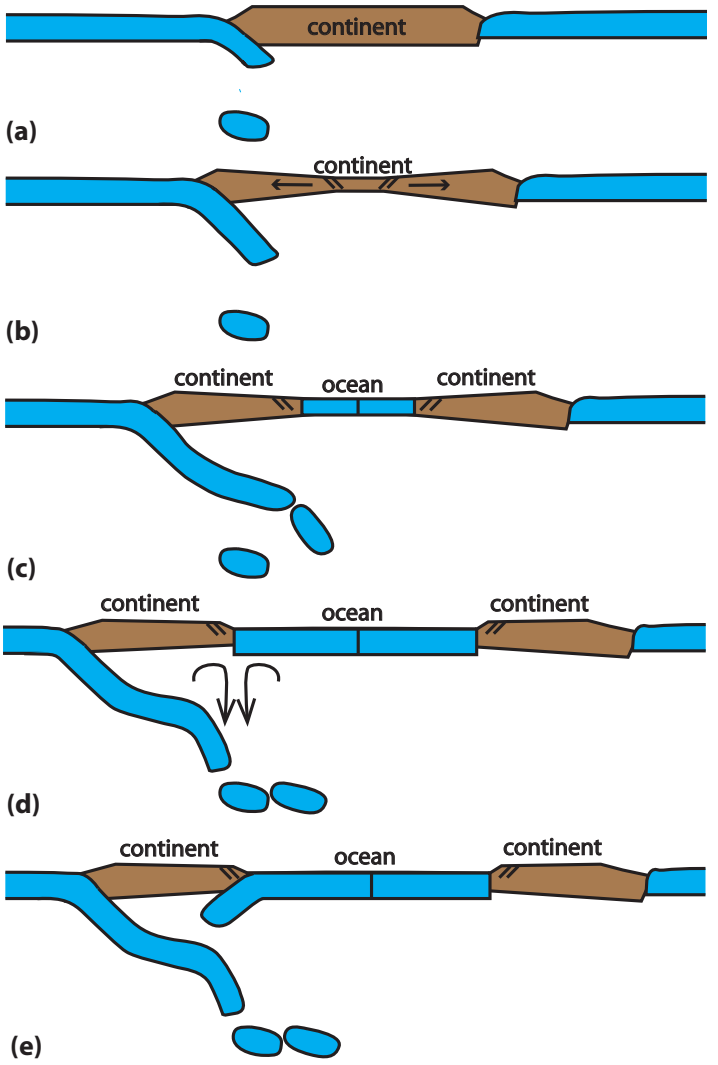

Figure 1. Modified scenario of the Wilson Cycle. (a) After rifting and (b) breakup of a continent, (c) a new oceanic basin forms. (d) The deep slab of neighboring subduction zones, along with slab remnants of the former converging plate boundaries in the midmantle, produces mantle suction flow, (e) which can break the passive margin and form a new subduction zone. In this scenario, the weakness of the continental crust, inherited from the rifting phase (shown with inclined lines near the passive margin), and the far-field topography within the continental plate, facilitate subduction initiation.

Cascadia, and Andean subduction zones, or from the remnants of the Farallon and Phoenix slabs in the midmantle. Based on this hypothesis, we suggest a modified version of the Wilson Cycle concept (Figure 1). Rifting and continuing extension results in the formation of a new ocean basin between two continents (Figures 1a–1c). Meanwhile, slabs from neighboring subduction zones, along with slab remnants of former active subduction zones in the midmantle, produce a down-going mantle flow (Figure 1d), which may cause plate failure, and the formation of a new subduction zone (Figure 1e). In this scenario, the rift-inherited weakness of the passive margin, and the horizontal push force induced from the far-field topographic gradient (Marques et al., 2013) within the continent, facilitate and speed up the subduction initiation process.

We tested our hypothesis using 2-D numerical models. We investigated the possibility of subduction initiation, triggered by mantle suction flow along a passive margin. We also examined subduction nucleation, induced by mantle flow along a fracture zone in the mid-ocean. The effect of different parameters, such as location, magnitude and domain width of the mantle flow, strength of the crust near the passive margin, length of the continental lithosphere, topographic gradient within the continent, and rheology of the mantle, is explored in a series of experiments (supporting information Table S1).

2. Numerical Model

In this study, we developed a series of 2-D numerical models, with the visco-elasto-plastic rheology constrained by laboratory experiments (Table 1). Although mantel suction flow has important 3-D features, the first-order effects of this parameter can be captured by analyzing a 2-D cross section. We used a 2-D version of SLIM3D (Popov & Sobolev, 2008), which is a finite element code, based on the Arbitrary Lagrangian-Eulerian method, to solve the thermomechanically coupled conservation equations of momentum, energy, and mass. The governing equations in our models are

$$\alpha\frac{DT}{Dt}-\frac{1}{K}\frac{DP}{Dt}=\frac{\partial v_i}{\partial x_i},$$

$$\frac{\partial \sigma_{ij}}{\partial x_j}+\rho g_i=0, \tag{1}$$

$$\rho C_P\frac{DT_P}{Dt}=\kappa\nabla^2 T+\left(\dot{\varepsilon}_{ij}^{vs}+\dot{\varepsilon}_{ij}^{pl}\right)\tau_{ij}+A,$$

where σ_{ij} is the Cauchy stress tensor, ρ is density, g_i is gravity acceleration vector, C_P is heat capacity, T is temperature, P is dynamic pressure, T_P is potential temperature, t is time, κ is thermal conductivity, $\dot{\varepsilon}_{ij}^{vs}$ is ductile creep strain rate tensor, $\dot{\varepsilon}_{ij}^{pl}$ is plastic strain rate tensor, τ_{ij} is the Cauchy stress deviator, A is the volumetric heat source, α is the coefficient of thermal expansion, K is the bulk modulus, v_i is velocity vector, and D/Dt is the substantial time derivative. Law of summation on repeating indexes applies. The elastic, viscous, and plastic deformation are based on additive decomposition of the total deviatoric strain rate ($\dot{\varepsilon}$), expressed as

$$\dot{\varepsilon}_{ij}=\dot{\varepsilon}_{ij}^{el}+\dot{\varepsilon}_{ij}^{vs}+\dot{\varepsilon}_{ij}^{pl}=\frac{1}{2G}\hat{\tau}_{ij}+\frac{1}{2\eta_{eff}}\tau_{ij}+\dot{\gamma}\ \frac{\partial Q}{\partial \tau_{ij}}, \tag{2}$$

where G is the elastic shear modulus, $\hat{\tau}_{ij}$ is the objective stress rate, η_{eff} is the effective viscosity, τ_{ij} is the Cauchy stress deviator, $\dot{\gamma}$ is the plastic multiplier, and Q is the plastic potential function.

Table 1
Material Properties Used in Numerical Experiments

Parameter	Upper continental crust	Upper continental crust near boundary	Lower continental crust near boundary	Lower continental crust near boundary	Continental lithospheric mantle	Oceanic crust	Oceanic lithospheric mantle	Asthenosphere
ρ (kg m^{-3})	2,800	2,800	2,850	2,850	3,300	2,900	3,300	3,300
K (GPa)	650	650	630	630	1,290	650	1,290	1,290
G (GPa)	400	400	400	400	740	400	740	740
log (B_{Diff}) (Pa^{-1} s^{-1})					−8.96		−8.78	−8.96
E_{Diff} (kJ/mol)					335		375	335
V_{Diff} (cm^{-3}/mol)					4		2	4
log (B_{Disloc}) (Pa^{-1} s^{-1})	−17.295	(–17.295) to (–14.295)	−15.4	(–15.4) to (–12.4)	−20.699	−15.4	−16.602	−20.699
E_{Disloc} (kJ/mol)	154	154	356	356	470	356	532	470
V_{Disloc} (cm^{-3}/mol)	0	0	0	0	14	0	14	14
n	2.3	2.3	3.0	3.0	4.0	3.0	3.5	4.0
μ	0.4	0.1	0.4	0.1	0.4	0.02	0.4	0.4
C (MPa)	3.0	3.0	3.0	3.0	3.0	3.0	3.0	3.0
α (10^{-5} K^{-1})	3.0	3.0	2.7	2.7	3.0	2.7	3.0	3.0
C_p (J kg^{-1} K^{-1})	1,200	1,200	1,200	1,200	1,200	1,200	1,200	1,200
κ (W K^{-1} m^{-1})	2.5	2.5	2.5	2.5	3.2	2.5	3.2	3.2
A (μW m^{-3})	1.5	1.5	0.2	0.2	0	0.2	0	0

Note. In Table 1, ρ is density, K is the bulk modulus, G is the shear modulus, log (B_{Diff}) is the preexponential constant for diffusion creep, E_{Diff} is the activation energy for diffusion creep, V_{Diff} is the activation volume for diffusion creep, log (B_{Disloc}) is the preexponential constant for dislocation creep, E_{Disloc} is the activation energy for dislocation creep, V_{Disloc} is the activation volume for dislocation creep, n is the power law exponent for dislocation creep, μ is the friction coefficient, C is cohesion, α is thermal expansivity, C_P is heat capacity, κ is heat conductivity, and A is radiogenic heat production.

The ductile temperature/stress-dependent viscosity in our models simultaneously accounts for the two creep mechanisms of diffusion and dislocation, as follows:

$$\eta_{eff} = \frac{1}{2}\tau_{II}(\dot{\varepsilon}_{Diff} + \dot{\varepsilon}_{Disloc})^{-1}, \tag{3}$$

where τ_{II} is the stress norm defined as square root of the second invariant of stress deviator, and $\dot{\varepsilon}_{Diff}$ and $\dot{\varepsilon}_{dis}$ are the effective scalar strain rates, due to the diffusion and dislocation creeps, respectively, which are defined as

$$\dot{\varepsilon}_{Diff} = B_{Diff}\tau_{II}\exp\left(-\frac{E_{Diff} + PV_{Diff}}{RT}\right), \tag{4}$$

$$\dot{\varepsilon}_{Disloc} = B_{Disloc}(\tau_{II})^{n}\exp\left(-\frac{E_{Disloc} + PV_{Disloc}}{RT}\right), \tag{5}$$

in which B_{Diff} is the preexponential constant for diffusion creep, E_{Diff} is the activation energy for diffusion creep, V_{Diff} is the activation volume for diffusion creep, R is the universal gas constant, T is absolute temperature, B_{Disloc} is the preexponential constant for dislocation creep, E_{Disloc} is the activation energy for dislocation creep, V_{Disloc} is the activation volume for dislocation creep, and n is the power law exponent for dislocation creep. Brittle (plastic) deformation is incorporated using the Mohr-Coulomb failure model, with the yield surface defined as

$$F = \frac{1}{2}(\sigma_{max} - \sigma_{min}) + \frac{1}{2}(\sigma_{max} + \sigma_{min})\sin\ \varphi - c\ \cos\ \varphi \leq 0, \tag{6}$$

where σ_{max} and σ_{min} are the maximum and minimum principal stresses (negative in compression), φ is the material angle of friction, and c is cohesion.

The mechanical weakening mechanism used in this study is friction softening, which is responsible for localization of deformation, and the formation of faults (Brune et al., 2012; Popov & Sobolev, 2008). It is incorporated into our model by a dependency of the friction coefficient on the accumulated plastic strain. To avoid

grid distortion, remeshing was used, in which the particle-in-cell method is conducted to project material properties from the distorted grid to the new grid.

2.1. Reference Model

We considered three different setups as reference models to examine subduction initiation, triggered by mantle suction force, induced by (a) slab remnants of former active subduction zones in the midmantle (supporting information Figure S1a, and model M74 in supporting information Table S1); (b) slabs from neighboring active subduction zones (supporting information Figure S1b, and model M59 in supporting information Table S1); and (c) both slab remnants from former subduction zones, and slabs from active subduction zones in the vicinity of the passive margin (supporting information Figure S1c, and model M162 in supporting information Table S1). Our reference models have a 3,000 km width and a 400 km depth. We used time steps of 5 kyr, and let the model evolve for 100 Myr, which is much longer than the integration time used in previous studies. We reran most of the models 3 or 4 times to explore their stability (supporting information Tables S1 and S2).

In the reference models, an oceanic plate, consisting of a 7 km crust and a 63 km mantle lithosphere, is placed on the right side of the model. On the left side is continental lithosphere, containing a 25 km lower crust, a 10 km upper crust, and a 65 km lithospheric mantle (supporting information Figure S1a). Below the oceanic and continental plates lies the asthenosphere, extending to a depth of 400 km. The continental lithospheric mantle and the asthenosphere were modeled as hydrous olivine, and the oceanic lithospheric mantle has a dry olivine rheology (Hirth & Kohlstedt, 2003). The upper and lower crustal layers deform in accordance with the naturally wet quartz (Gleason & Tullis, 1995) and wet anorthite (Rybacki & Dresen, 2000) laws, respectively. The material properties of the different model layers are listed in Table 1. We introduced a very low friction coefficient (0.02) for the oceanic crust, to lubricate the plate interface as the oceanic plate starts to sink into the mantle. The weakness of the continental crust, inherited from the rifting phase near the plate interface, was approximated by a low friction coefficient of 0.1 and, in some models, by a lower preexponential constant for dislocation creep (reduction of B_{Disloc} in equation (5)) for continental crust near the passive margin (supporting information Table S1). We investigated the effect of strength of continental crust near the margin in a series of experiments (models M89–161 and M165-M170, supporting information Table S1). The friction coefficient for the rest of the model was set to 0.4. The far-field topographic gradient within the continental plate was modeled by the incorporation of a thicker, 45 km, continental crust and a thicker, 120 km, thermal lithosphere, in the first 200 km, on the left side of the model.

The top boundary of the model is a free surface with zero stress. The lower boundary is free slip, except in the center and/or the left side, where we imposed velocities or forces to simulate mantle suction flow. For instance, in reference model M74, we imposed a velocity field of 1,000 km, in the middle of the lower boundary, with a maximum of 2 cm/yr in the center, decreasing to zero toward the side boundaries (supporting information Figure S1a). In reference model M59, a velocity field with maximum of 4 cm/yr (average of 2 cm/yr) was imposed on the first 600 km of the left side of the lower boundary, decreasing to zero toward the right side of the model (supporting information Figure S1b). In reference model M162, two velocity fields, with the domain size of 600 km, were imposed on the center and left side of the model's lower boundary, with maximum velocities of 2 and 4 cm/yr, respectively (supporting information Figure S1c). The assumed magnitude of mantle flow velocities in our models is in good agreement with the estimates of slab sinking velocities in the upper mantle, transition zone, and lower mantle (Becker & Faccenna, 2011; Goes et al., 2008). The right boundary was opened, allowing the net inflow and outflow to stay in balance. The left boundary was a free slip boundary.

The initial temperature field for the oceanic plate was defined based on the cooling half space (Turcotte & Schubert, 1982). The surface temperature in the right side of the model was 1,350°C, simulating temperature at mid-oceanic ridge. Temperature was decreased toward the passive margin as a result of cooling of the oceanic plate. We considered a half spreading velocity of 2.0 cm/yr, a typical half spreading rate of Atlantic mid-oceanic ridge (Conrad & Lithgow-Bertelloni, 2007). Near the passive margin, the temperature field of the oceanic plate simulated temperature of an 80 Myr oceanic lithosphere. Considering an oceanic plate, which was cooling down from mid-oceanic ridge toward the passive margin, enabled us to explicitly include ridge push force in our models. In the continental plate, the temperature was incorporated by a

steady state geotherm, with a surface temperature of 0°C, and a temperature of 1,200°C at the base of the lithosphere.

2.2. Alternative Numerical Model Setups

We conducted a series of experiments to analyze the sensitivity of the results to different parameters (supporting information Tables S1 and S2). The initial setups of some of our experiments are shown in supporting information Figure S1. Below, we explain the model description for exploring spontaneous subduction initiation, subduction nucleation induced by mantle flow under the U.S. East Coast and along fracture zones in the middle of the ocean, and formation of a new subduction zone in a collisional setting. We also briefly describe the model setup of experiments with no far-field topographic force within the continent, and models with different mantle rheologies.

2.2.1. Spontaneous Subduction Initiation

To explore the possibility of spontaneous subduction initiation, we established a model similar to the reference models (M59, M74, and M162), except that, here no mantle flow was imposed on the base of the model. Therefore, the whole model base is a free slip boundary (supporting information Figure S1d). In this model, no external forces were involved in the system, and the only governing force is the gravitational (body) force, whereas the same margin weak zone and far-field high topography were implemented in the lithosphere as in the reference models.

2.2.2. Subduction Initiation Under the U.S. East Coast

The length of the continental lithosphere, and height of the far-field topography, in our reference models are in accordance with those in the Argentine passive margin. Since the continental length and height of the Rocky Mountains are larger than those in the Argentine passive margin, we conducted some experiments with different model setups to explore subduction initiation along the U.S. East Coast (models M159-M161, supporting information Table S1). The initial model setup is shown in supporting information Figure S1e. This model is similar to the reference model, except that the continental lithosphere is 2,000 km longer, and the far-field topography is approximately 900 m higher. The higher far-field topography was incorporated by a thicker (50 km) continental crust in the first 200 km in the left side of the model. We investigated the effect of the magnitude of mantle suction flow velocity in models M159-M161 (supporting information Table S1).

2.2.3. Subduction Initiation in a Collisional Setting

In some of our models, we explored the initiation of subduction due to external compressional forces. In these models, instead of imposing of a mantle suction flow at the base of the model, a convergence rate was imposed on the continental lithosphere (supporting information Figure S1g). For instance, in model M157 (supporting information Table S1), we imposed a convergence velocity of 3 cm/yr—the rate of convergence between India and Eurasia—on the continental lithosphere, to simulate the compressional stress induced by continental collision. In this model, the upper 50 km of the right boundary was fixed, and the right and left boundaries below 50 km, and the lower boundary, were open.

2.2.4. Subduction Initiation Along Fracture Zones in the Middle of the Ocean

Previous modeling studies on subduction initiation along transform faults/fracture zones (Gurnis et al., 2004; Hall et al., 2003; Leng & Gurnis, 2015; Toth & Gurnis, 1998) have indicated the implausibility of spontaneous subduction initiation and, hence, the necessity of an extra force to trigger subduction nucleation. In those studies, a convergence velocity, or force, was imposed on the oceanic lithosphere to facilitate subduction initiation. Here we explored the possibility of subduction nucleation along fracture zones due to the extra force induced from mantle suction flow. To this end, we set up a series of models (supporting information Table S2) in which an oceanic lithosphere is separated from the asthenosphere by a vertical weakness zone in the lithospheric level (supporting information Figure S1h). These models simulated a cross section, cutting the ocean near to, and parallel with, the mid-oceanic ridge, similar to the model setup of (Hall et al., 2003). The weakness zone, simulating a fracture zone, has a constant viscosity of 1×10^{19} Pa s, which is the minimum viscosity in the model. We conducted a series of experiments in which the effect of mantle rheology, the age of the oceanic lithosphere, and different mantle suction flow velocities were investigated (supporting information Table S2).

2.2.5. The Effect of a Far-Field Topographic Gradient Within the Continent

To investigate this effect, we set up models with different far-field topographies (models M155 and M156). The setup of M156 is similar to model M74, except that here, the continental crust and lithosphere on the left side of the model are not thicker than the other parts of the continent (supporting information Figure S1f). The mantle flow in this model was simulated by imposing a velocity field with a domain size of

1,200 km in the middle of the model, with a maximum of 6 cm/yr, decreasing toward the sides of the model. The other difference between this model and model M74 is the strength of the continental crust near the margin. In this model, the crust is stronger near the margin, compared to the one in model M74. Model M155 is different from model M156 in that it has a far-field topography that is higher than that in model M74. In this model, compared to model M74, a thicker continental crust (50 km) and a thicker thermal lithosphere (130 km) were considered in the first 200 km of the left side of model.

2.2.6. The Effect of Water in the Mantle

As there are some uncertainties in the amount of water in the upper mantle (Fei et al., 2013; Karato et al., 1986), we established some experiments to investigate the influence of wet and dry olivine rheology on the results (models M147-M153, supporting information Table S1). The model setup is similar to that of the reference models, but here we considered wet or dry olivine rheology for different parts of the mantle in different models.

3. Model Results

3.1. Spontaneous Subduction Initiation

The model outcomes of the experiment with no suction flow (model M1 in supporting information Table S1) indicate that no significant deformation occurs, even after 100 Myr (Figure 2a). This confirms previous modeling results concerning the stability of a passive margin with a realistic lithospheric structure (Cloetingh et al., 1982, 1984, 1989; Nikolaeva et al., 2010). It also demonstrates that the inherited weakness of the rifted crust, and the wet olivine rheology of the continental lithospheric mantle, as well as the realistic far-field topography within continent and ocean, do not change this conclusion. Note that, as we have a mid-ocean ridge at the right boundary of our model (supporting information Figures S1a–S1f), the ridge push force is automatically considered; however, it is not sufficient to initiate subduction at the passive margin.

3.2. Subduction Initiation Triggered by Mantle Suction Flow Induced by Neighboring Subduction Zones

The model with mantle suction flow induced by a neighboring subduction zone (reference model M59, supporting information Table S1) shows that mantle suction flow inspires shear stress at the base of the

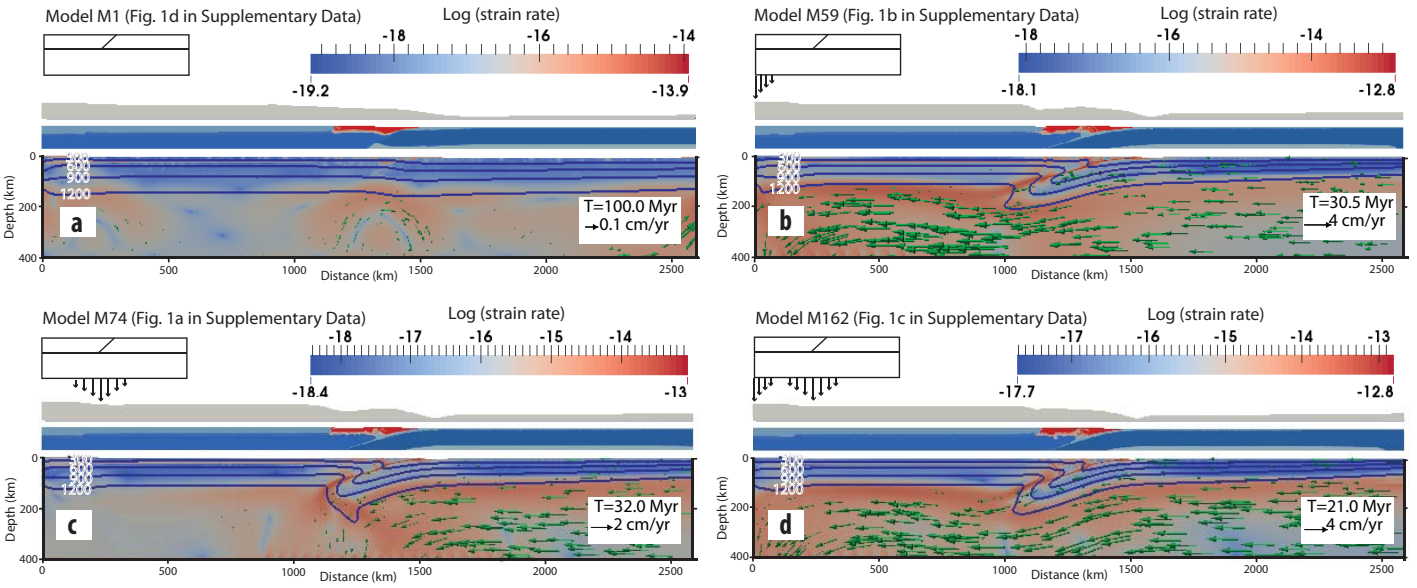

Figure 2. Results of reference models, along with a model exploring spontaneous subduction initiation. (a) Results of model M1 (supporting information Table S1) in which no mantle flow is imposed demonstrating that subduction cannot be initiated spontaneously. (b–d) Results of reference models M59, M74, and M162, respectively (supporting information Table S1), showing that, in the presence of sufficiently strong mantle suction flow, subduction can be initiated. (top left) Illustrates the location of suction flow; (bottom) illustrates: (top) exaggerated surface topography, (middle) the material phase field of the upper 90 km of the model, and (bottom) the logarithm of the strain rate field, along with velocity vectors and temperature isoclines. (middle) The red-colored and orange-colored areas near the margin indicate the rift-inherited weakness zone in the continental crust. The light blue-colored regions in the upper parts of the left and right sides of the middle figure correspond to upper continental and oceanic crust, and the dark blue-colored areas refer to the lithospheric mantle.

lithosphere, resulting in compression of the passive margin (Figure 3). The weak, and gravitationally unstable, continental crust starts to thrust over the oceanic plate. As a result, a shear zone slowly forms in the upper part of the lithosphere, near the plate interface (Figure 3a). This overthrusting of continental crust results in extension in continental crust near the margin. At the same time, a depression in the surface topography forms along the passive margin, indicating the future trench location. With time, the shear zone cuts through the entire lithosphere, and the oceanic plate begins to gradually descend into the mantle, driven by the shear stress imposed by the mantle flow along this shear zone (Figures 3b and 3c). Simultaneous continental crust overthrusting and oceanic plate underthrusting continue, and the surface depression deepens. Self-sustaining subduction is initiated at approximately 30.5 Myr, and is accompanied by continuous spreading of the continental crust over the oceanic plate (Figures 2b and 3d).

The magnitude of lithosphere basal shear stresses, caused by mantle flow, in the model is about 1.5 MPa (supporting information Figure S2). That integrates to the additional force of about 2×10^{12} Pa m, which is similar to the ridge push force.

3.3. Subduction Initiation Triggered by Mantle Suction Flow Induced by Slab Remnants From Former Subduction Zones

Sufficiently extensive mantle suction flow just below the continental margin forces the margin to break. The deformation pattern of the reference model (M74), in which velocities are imposed at the middle of the lower boundary (Figure 2c), is very similar to that of the reference model, with suction flows coming from a neighboring subduction zone (M59), except that, here there is less prominent mantle flow below the continent (compare Figures 2b and 2c). This may result in the formation of a more steeply dipping subduction zone.

3.4. Subduction Initiation Triggered by Mantle Suction Flows Induced by Neighboring Subduction Zones and Slab Remnants From Former Subduction Zones

The main difference between the results of reference model M162, simulating mantle suction flows coming from both active and former subduction zones, and the two other reference models (M59 and M74) is in the flow pattern in the asthenosphere, which may affect the dip angle of the developing subduction zone.

3.5. Subduction Initiation in a Collisional Setting

If the mantle suction force is not sufficient to break a passive margin, it will survive for a long time; however, the ocean at the active subduction side of the continent will close at some point, leading to continent-continent collision. In this case, the continent with the passive margin will be subjected to external compressional forces. Our experiments (models M157 and M158) demonstrate that, in this case, the passive margin can be converted into a subduction zone, after a rather short period of convergence. For instance, with the convergence rate of 3 cm/yr, similar to the present-day convergence rate between India and Eurasia, subduction is initiated after only 8 Myr (Figure 4).

3.6. The Effect of Side Boundary Conditions, and Depth of the Model

In reference model M74, the left boundary is a free slip boundary. We examined the effect of boundary conditions on the results by setting up a model similar to M74, but with both right and left boundaries open below the depth of 100 km. In this model, the uppermost 100 km of the left boundary is a free slip boundary. The evolution of deformation for this model, and model M74, are shown in supporting information Figures S3a–S3c and S3d–S3f, respectively. As seen from this figure, the flow pattern in the beginning is different in the two models, which is a result of the implementation of different boundary conditions; however, as soon as the shear zone cuts through the entire lithosphere, and the oceanic lithosphere starts to sink into the mantle, the flow from the right boundary becomes the dominant flow in the model. The flow pattern in both models becomes very similar afterward. The time of subduction initiation differs slightly between these models. The results of this model indicate that our choice of boundary conditions for lateral boundaries has a negligible effect on the results.

We also set up some models with a greater depth of 660 km, to investigate the effect of depth of the lower boundary on the results (supporting information Table S3). Supporting information Figures S4 and S5 show the results of two models, similar to reference models M59 and M75, but with a base at 660 km depth. The results do not change much when the model base is deeper (660 km instead of 400 km), although we do need a slightly longer time for subduction initiation—45 Myr in model MM59

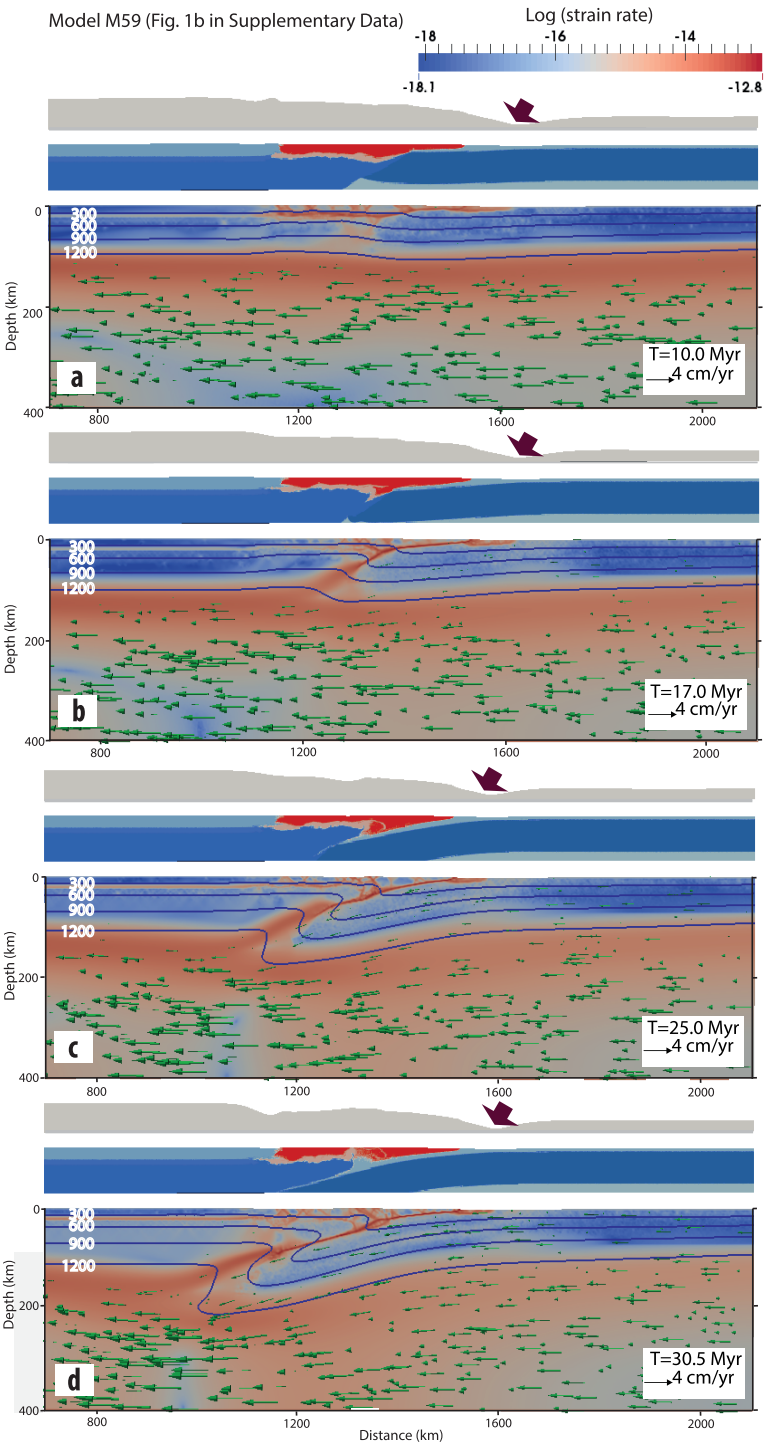

Figure 3. Reference model M59 results. The three plots in (a–d) show: (top) exaggerated surface topography, (middle) the material phase field of the upper 90 km of the model, and (bottom) the logarithm of the strain rate field, along with velocity vectors and temperature isoclines. (middle) The red-colored and orange-colored areas near the margin indicate the rift-inherited weakness zone in the continental crust. The light blue-colored regions in the upper parts of the left and right sides of the middle figure correspond to upper continental and oceanic crust, and the dark blue-colored areas refer to the lithospheric mantle. Red arrows point at the location of the (future) trench. (a) At t = 10 Myr, a shear zone develops along the margin, cutting the upper parts of the lithosphere, and a depression develops in the surface topography. At this time, continental crust starts to thrust over the oceanic plate. (b) As the shear zone cuts through the entire lithosphere, the oceanic plate starts to sink into the mantle. (c) The oceanic plate bends downward. (d) Subduction is initiated at approximately 30.5 Myr. In Figures 3b–3d, the depression in the surface topography near the margin deepens, and overthrusting of the continental lithosphere continues.

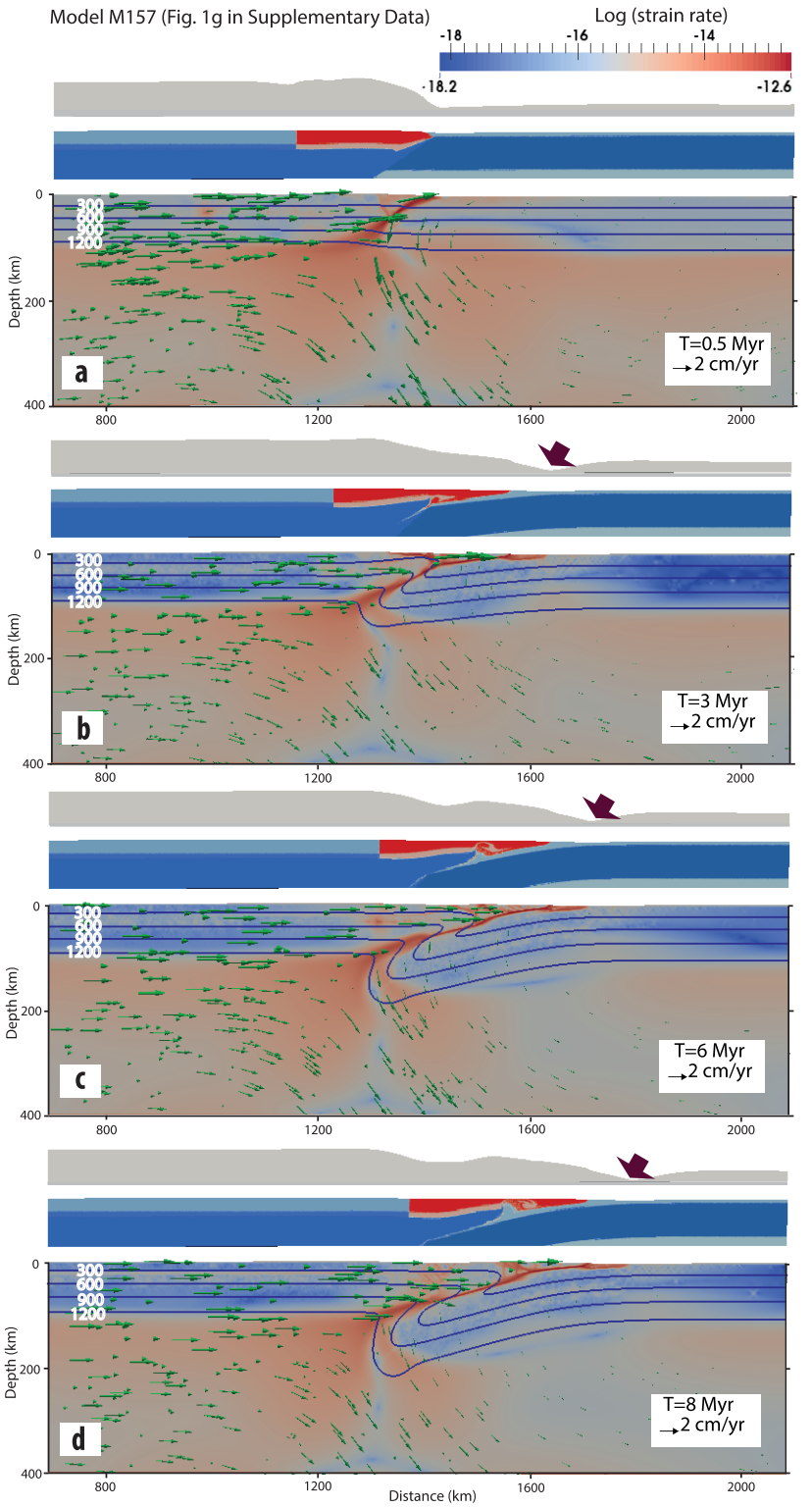

Figure 4. Model results for subduction initiation in a collisional setting (see initial setup in supporting information Figure S1g). Here we aimed to investigate the following scenario: in the extreme case of the continuous spreading of the Atlantic Ocean, which leads to closure of the Pacific Ocean, collision between the American and Eurasian plates occurs. This imposes a compressional force on the continental lithosphere, helping to convert the Atlantic passive margin into a subduction zone. (a–d) Results of model M157 (supporting information Table S1), in which a convergence velocity of 3 cm/yr is imposed on the oceanic lithosphere. Subduction is initiated at 8 Myr. For description of the figures, see Figure 3.

(supporting information Table S3), instead of about 30 Myr in model M59 (supporting information Table S1)—or a wider sinking domain—1,200 km in model MM75 (supporting information Table S3), instead of 1,000 km in model M74 (supporting information Table S1). The reason for this insignificant change is that the horizontal mantle flow is mostly concentrated in the upper 300–400 km of the mantle, where viscosity is lower.

3.7. Sinking Block Instead of Kinematic Boundary Conditions

We set up a model with a depth of 1,000 km, in which a detached slab is located at a depth of 400 km (similar depth to the base of reference model). In this model, the upper 150 km of the left boundary is fixed in both the *X* and *Y* directions, and 700 km of the left and right sides of the lower boundary are free slip. The other parts of the left, right, and lower boundaries are open. Supporting information Figure S6 shows the results of two models, with different slab temperatures of 1,000°C (Figures S6a–S6c) and 800°C (Figures S6d–S6f). As inferred from the figure, the results of these models are very similar to the reference model, indicating that kinematic boundary conditions at a depth of 400 km can simulate suction mantle flow, induced by sinking slabs, reasonably well.

3.8. The Effect of Crustal Strength Near the Passive Margin

In our reference models, the weakness of the continental crust near the passive margin, which was inherited from the rifting phase, was modeled by considering a lower internal friction of 0.1, and a 3 orders of magnitude reduction in the preexponential constant of dislocation creep (reduction of B_{Disloc} in equation (5)). The outcomes of models similar to M74, but with stronger continental crust near the passive margin (no reduction of the preexponential constant of dislocation creep), demonstrate that subduction initiation is possible only if a stronger mantle flow, compared to that in model M74, exists below or near the passive margin (models M89-M146 in supporting information Table S1). Experiments with mantle flow coming from neighboring subduction zones indicate that a minimum reduction of 1.5 orders of magnitude in the preexponential constant of dislocation creep is needed to trigger subduction initiation along a passive margin (models M168-M170, supporting information Table S1).

3.9. The Effect of the Strength and Location of Mantle Suction Flow

The possibility and timing of subduction initiation depends on several parameters, such as the magnitude, location, and domain width of the mantle suction flow (supporting information Table S1). In the case of mantle flow mainly induced by the slab remnants of former subduction zones, the optimum location for the center of a mantle suction flow with small domain width and magnitude to trigger subduction initiation is exactly below the passive margin (Figure 5). For a larger domain width and a stronger mantle flow, however, subduction can be initiated, even if the center of mantle suction flow is significantly displaced, relative to the passive margin (Figures 5, 6b, and 6d). In general, models with mantle flow induced by both neighboring subduction zones, and slab remnants of former active margins, show similar behavior (Figure 6). When the effective width of mantle suction flow is narrow, subduction initiation is possible only if the mantle flow is strong. In contrast, when the mantle suction flow extends over a large area, a moderate flow is able to trigger subduction initiation at a passive margin.

3.10. Formation of a New Subduction Zone Along a Fracture Zone in Mid-Ocean

Our models simulating fracture zones in mid-ocean (supporting information Table S2) without any suction force resulted in similar behavior to that found by previous studies (Gurnis et al., 2004; Hall et al., 2003), indicating that, in the absence of mantle suction flow, spontaneous subduction initiation cannot be achieved, even after a model time of 90 Myr (Figure 7a). However, with a moderate mantle flow (velocity of 2–3 cm/yr), subduction is readily initiated in less than 15 Myr (Figures 7b–7d).

3.11. The Effect of Water in the Mantle

Results of models with different mantle rheologies (models M147-M153 in supporting information Table S1) show that subduction is initiated only if the continental lithospheric mantle has a wet olivine rheology. This indicates that water penetration into the lithosphere from past subduction zones (van der Lee et al., 2008) is a critical condition in conversion of passive margins into active ones.

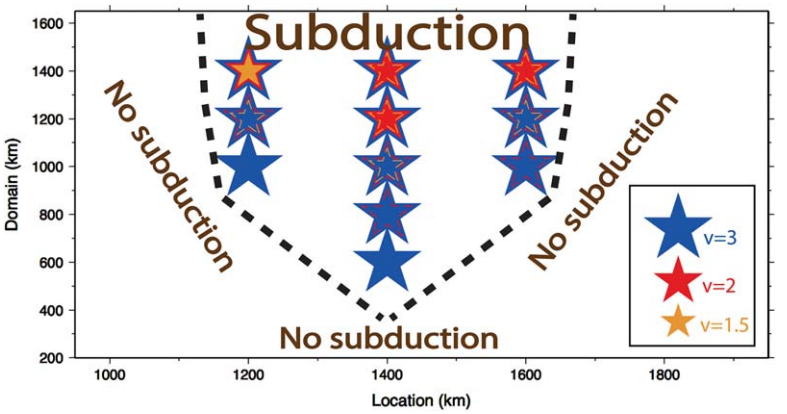

Figure 5. Results of models with suction flow affecting the regions near the passive margin (mainly induced by slab remnants of former subduction zones) with different magnitudes, domain widths, and locations of mantle suction flow. Different colors stand for different average mantle flow velocities of 3, 2, and 1.5 cm/yr. Dashed stars refer to models with unstable results (see supporting information Table 1S). The passive margin in all models is located at 1,400 km. Models show that, if mantle suction flow is narrow ($\leq$800 km), then subduction is initiated only if the mantle flow velocity is high ($v \geq 3$ cm/yr), and the flow is centered exactly below the passive margin. Subduction initiation can occur with a moderate mantle flow velocity ($v < 3$ cm/yr) when the mantle flow extends to a broader zone ($>$800 km), which does not have to be centered below the margin.

4. Discussion

Using numerical models, we have shown that subduction initiation at a passive margin, which is a key component of the Wilson Cycle in its closing phase, is possible despite the high strength of passive margins. This requires an additional forcing, provided by mantle flow induced by neighboring subduction zones and/or by midmantle slab remnants (Figure 6). We emphasize that our intention here was not to focus on the formation of the first subduction zone, and the beginning of plate tectonics. Our aim in this study was to investigate how new subduction is formed, and how the Wilson Cycle may work in present-day tectonic settings. Therefore, we have assumed the preexisting subduction zones in our scenario for a modified version of the Wilson Cycle (Figure 1). Our successful models show that weakness of the continental crust, inherited from the rifting phase near the plate interface is essential for subduction initiation. In these models overthrusting of continental crust and extension of the continental plate near the future plate boundary precede subduction initiation. This is in agreement with previous studies (Kemp & Stevenson, 1996; Nikolaeva et al., 2010), indicating that subduction initiation along passive margins is accompanied by a tensile regime in the continental crust near the plate interface.

The results of models with different far-field topographies imply that a topographic gradient within the continental plate facilitates subduction nucleation (models M155-M156 in supporting information Table S1). This is in accordance with previous studies, suggesting an extra push force, such as a ridge push force (McKenzie, 1977), or a far-field topographic force (Marques et al., 2013), facilitates subduction initiation. Numerical experiments with dry olivine rheology for the mantle part of the continental lithosphere failed to initiate subduction, even with prescribed mantle suction flow (models M147-M150 in supporting information Table S1). This suggests that a weakened mantle lithosphere is required for subduction initiation, and water infiltration into the lithosphere from past subduction zones is one possible mechanism (van der Lee et al., 2008).

Our experiments show that the magnitude of mantle suction flow and the strength of continental crust near the passive margin required to trigger subduction initiation depend on the location of the mantle flow (Figure 6). When the mantle flow, which is most likely induced by slab remnants from former subduction zones, is below or near the passive margin, a weaker flow can initiate a subduction zone with a stronger continental crust near the margin, compared to the case where mantle flow is derived from neighboring subduction zones. Models in which mantle suction flow originated from neighboring subduction zones indicate that a reduction of at least 1.5 orders of magnitude in the preexponential constant of dislocation creep for continental crust near the margin is needed to convert a passive margin into a converging plate

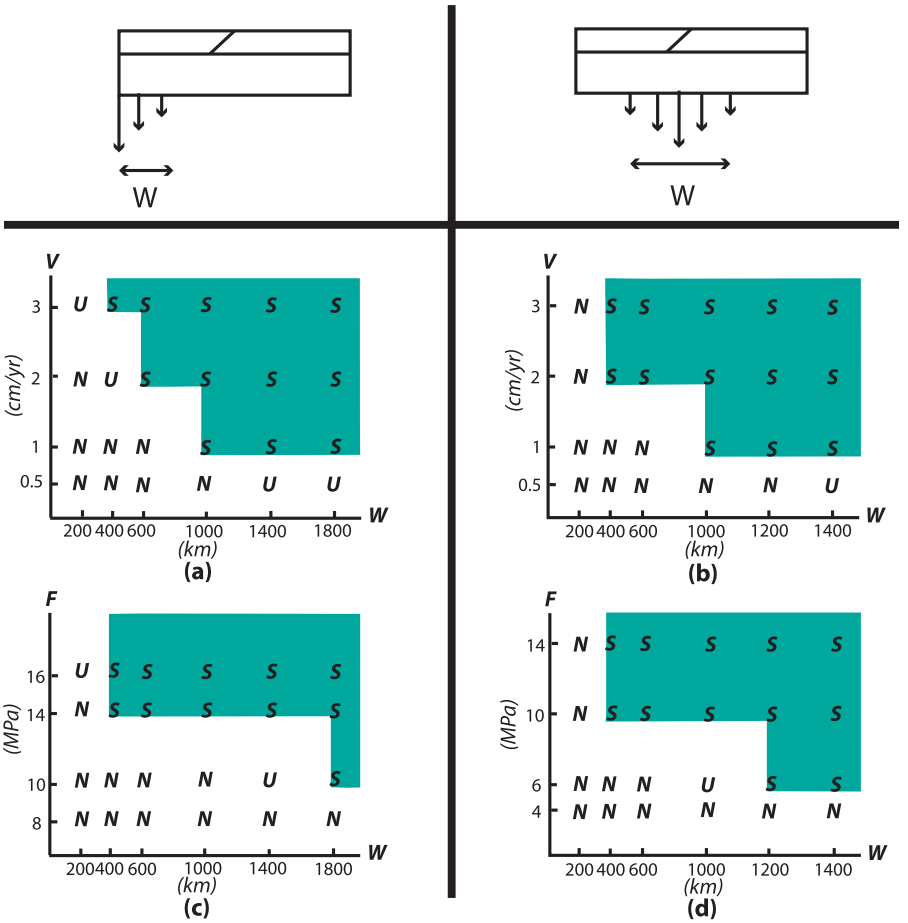

Figure 6. Results of models with (a, b) kinematic or (c, d) dynamic boundary conditions, with different magnitudes and domain widths of mantle suction flow. Schematic figures in the top figures show the location of imposed velocity or force in the model, which can be either (left) on the left side or (right) in the middle of the bottom lower boundary. In Figures 6a–6d, V, W, F, U, S, and N indicate magnitude of velocity boundary conditions, width of imposed boundary conditions, magnitude of force boundary conditions, unstable situation, subduction initiation, and no subduction initiation, respectively. The magnitude of velocity on the vertical axis in Figures 6a and 6b is the average velocity in cm/yr. The green areas in Figures 6a–6d indicate the areas where mantle suction flow can trigger subduction initiation. (a, b) Results of models in which different magnitudes of velocity, with different widths, are imposed on the (a) left and (b) middle of the lower boundary. (c, d) Results of models in which different magnitudes of force, with different widths, are imposed on the (c) left and (d) middle of the lower boundary.

boundary. This amount of weakening along a passive margin is consistent with the findings of (Brune et al., 2014) on the reduction of the strength of the continental crust near the margin during the rifting phase.

The time of subduction initiation in most of our experiments is more than 20 Myr, suggesting that subduction nucleation at passive margins is a long-term process, compared to subduction initiation in other tectonic settings, such as transform faults/fracture zones and mid-ocean ridges, which occurs in a few million years (Gurnis et al., 2004; Hall et al., 2003; Toth & Gurnis, 1998). In addition, the three-dimensionality of the passive margins, that was neglected in our 2-D models, increases the resistance to subduction, further increasing the subduction initiation time. The long-term process of subduction initiation can explain the absence of any Cenozoic conversions of a passive margin into an active one; however, an interesting question is where may the next conversion of a passive margin into an active subduction zone be expected in the future?

We propose that, along the Atlantic passive margins, there are at least two locations where subduction initiation may be triggered by mantle suction flow. One candidate location is the Argentine Basin, located in the southern part of South America, which is considerably deeper than would be expected from the age of the oceanic lithosphere. The present-day dynamic surface topography shows that the Argentine Basin exhibits one of the largest negative dynamic topography signals in the world, reaching up to 1 km (Flament et al., 2013; Steinberger, 2007). This points to the existence of a large mantle downwelling in this region,

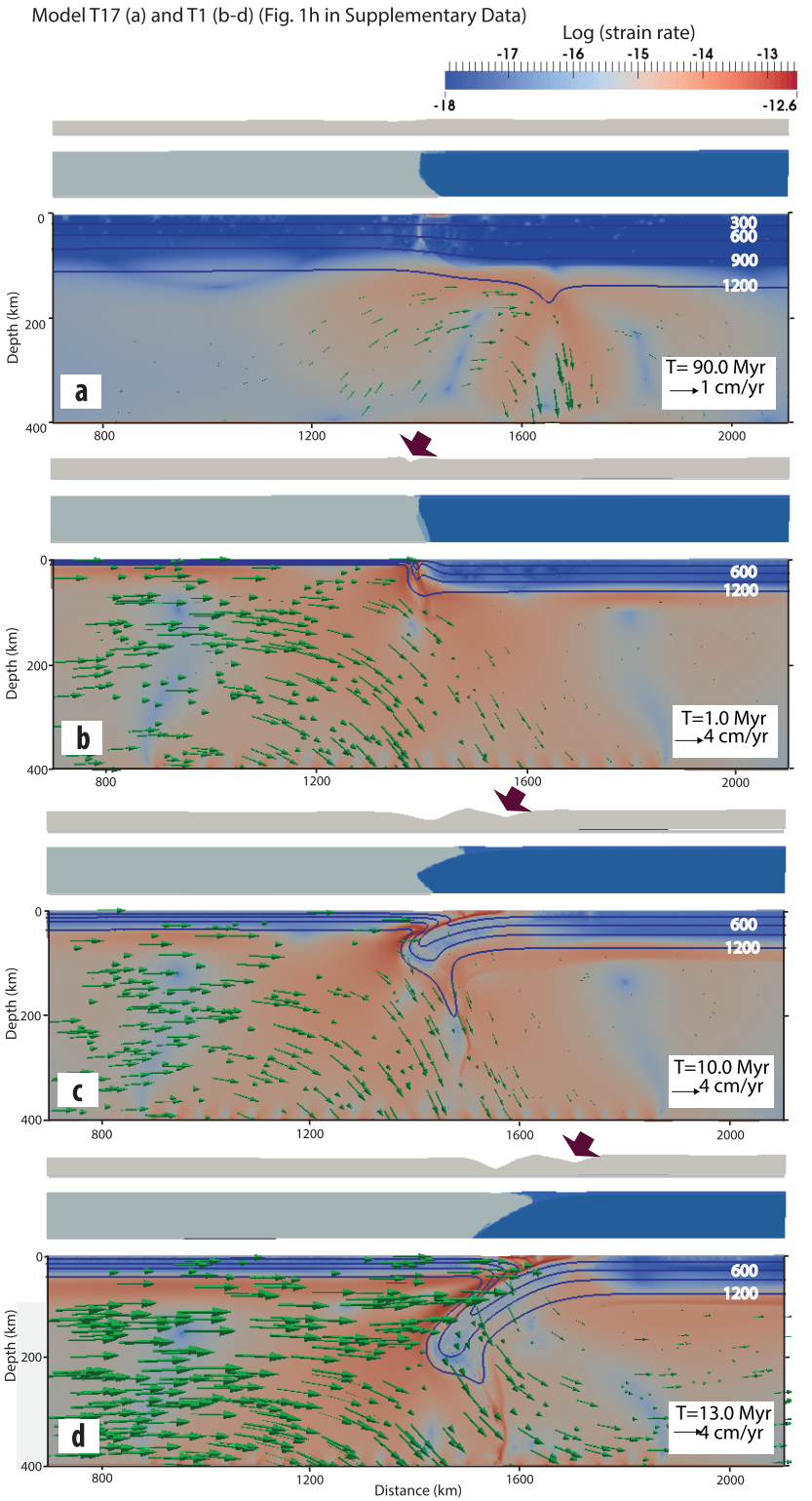

Figure 7. Model results for subduction initiation along a fracture zone in the middle of the ocean (see initial setup in supporting information Figure S1h). (a) Results of model T17 (supporting information Table S2), in which no mantle suction flow is imposed on the model. No significant deformation occurs after 90 Myr, indicating that subduction cannot be initiated spontaneously along a fracture zone. (b–d) Results of model T1 (supporting information Table S2). This model differs from model T17 in that a mantle suction flow with an average velocity of 2 cm/yr is imposed on the middle of the lower boundary. In this model, subduction nucleates at approximately 13 Myr. For description of the figures, see Figure 3.

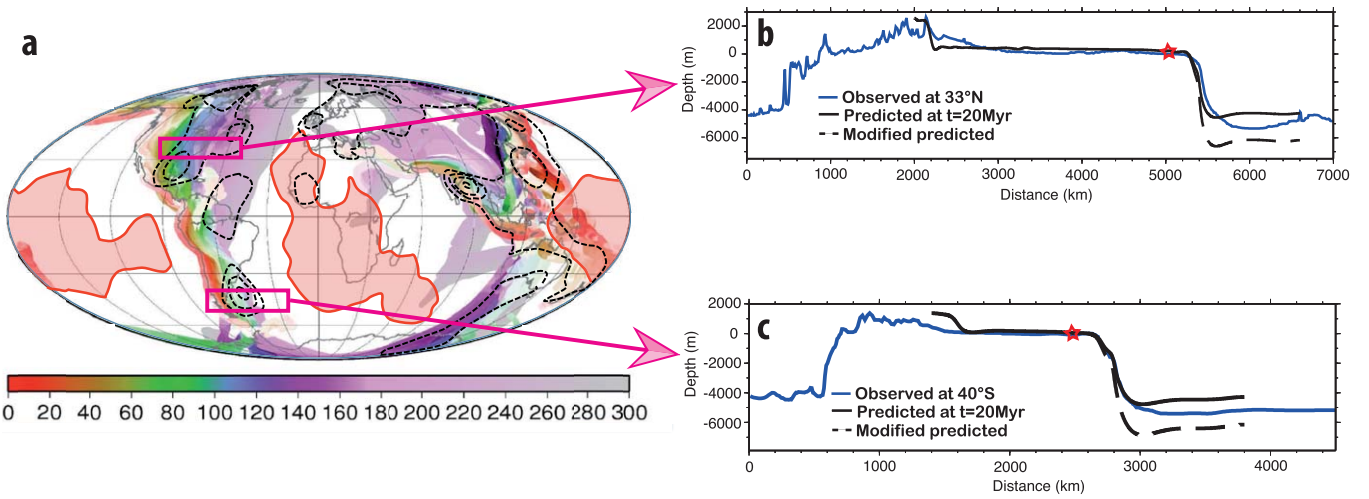

Figure 8. (a) Distribution of past subduction zones, with colors corresponding to their ages in Myr. (Steinberger, 2007). Pale rose-colored domains show two major LLVSPs (Large Low Shear Velocity Provinces) (Seton et al., 2012), and dashed black contours denote the largest depressions in dynamic topography (Flament et al., 2013). Pink rectangles show two locations along the Atlantic passive margin where subduction initiation is likely to be triggered by mantle suction flow. (b) Surface topography of the U.S. East Coast passive margin. The blue curve indicates the DEM data from ETOPO5 (Noaa, http://oos.soest.hawaii.edu/erddap/griddap/etopo5.html) at 33°N. The two black curves show the model-predicted surface topography at 20 Myr, with (dashed curve), and without (solid curve) isostatic correction for water load. The red star shows the location of the 2011 Virginia Mw 5.8 earthquake. (c) Surface topography in the Argentine passive margin. The blue curve indicates the DEM data from ETOPO5 (Noaa, http://oos.soest.hawaii.edu/erddap/griddap/etopo5.html) at 40°S. The description of the black curves is similar to those in Figure 8b. The red star shows the location of the 2011 Mw 4 earthquake.

most likely related to the sinking slabs of the Phoenix, Farallon, and Nazca Plates (Shephard et al., 2012). This is confirmed by global tomographic images (Bijwaard et al., 1998; Shephard et al., 2012), showing high *P* wave velocity bodies, both in the upper and lower mantle beneath eastern Argentina. The narrow continental plate in this region also facilitates transformation of the mantle flow, induced by the Andean subduction zone in the western part of South America into the eastern part. There is some seismic activity at this continental margin. According to the USGS earthquake catalog, an earthquake with a magnitude of Mw 4 occurred at 10 km depth at 40.2°S, 57.9°W in 2011. Additionally, DEM data from ETOPO5 (Noaa, http://oos.soest.hawaii.edu/erddap/griddap/etopo5.html) show a depression in the surface topography along the Argentine passive margin, at latitudes between 40°S and 45°S. We propose that the evidence from dynamic topography, the tomographic images, and the DEM data are all indicative of the earliest phase of formation of a new converging plate boundary along the Argentine passive margin at latitudes between 40°S and 45°S. The extra push force induced from the Southern Andes, uplifted during the last 5 Myr (Vietor & Echtler, 2006), should facilitate subduction nucleation in the Argentine Basin. We have found that the DEM data (Noaa, http://oos.soest.hawaii.edu/erddap/griddap/etopo5.html) match well with the predicted model surface topography (model M139 in supporting information Table S1) at the failure phase of the top portions of the lithosphere ($t \approx 20$ Myr; Figure 8c), suggesting that subduction initiation in Argentina may be in the initial stage of shear zone formation in the upper parts of the lithosphere, and self-sustained subduction may be initiated in a few tens of millions of years.

Another possible location for conversion of a passive margin into a subduction zone is the U.S. East Coast, at latitudes of approximately 30°N–40°N. The Cascadia subduction zone, on the U.S. West Coast, and slab remnants of former subduction zones, such as the Laramide and Farallon slabs, which have been identified in seismic tomographic images below the U.S. continent at different depths (Bijwaard et al., 1998; Sigloch, 2011), produce some mantle suction flow under the U.S. East Coast. This is evidenced by the large negative anomaly in the vertical component of the mantle flow velocity field, at depths of 410 and 660 km below this area (Steinberger, 2007, Figure 5). According to the USGS earthquake catalogue, the U.S. East Coast is tectonically active, as some small to moderate earthquakes have hit the region. The Mw 5.8 earthquake of 23 August 2011, near Mineral, Virginia, was the largest earthquake in the central and eastern U.S. in the past 100 years (Li et al., 2014), and it was unusually large for occurring close to a passive margin. We attribute this earthquake to the formation of a new converging plate boundary along the U.S. East Coast. The model results of experiment M160 (supporting information Table S1) show that, because of the larger length of

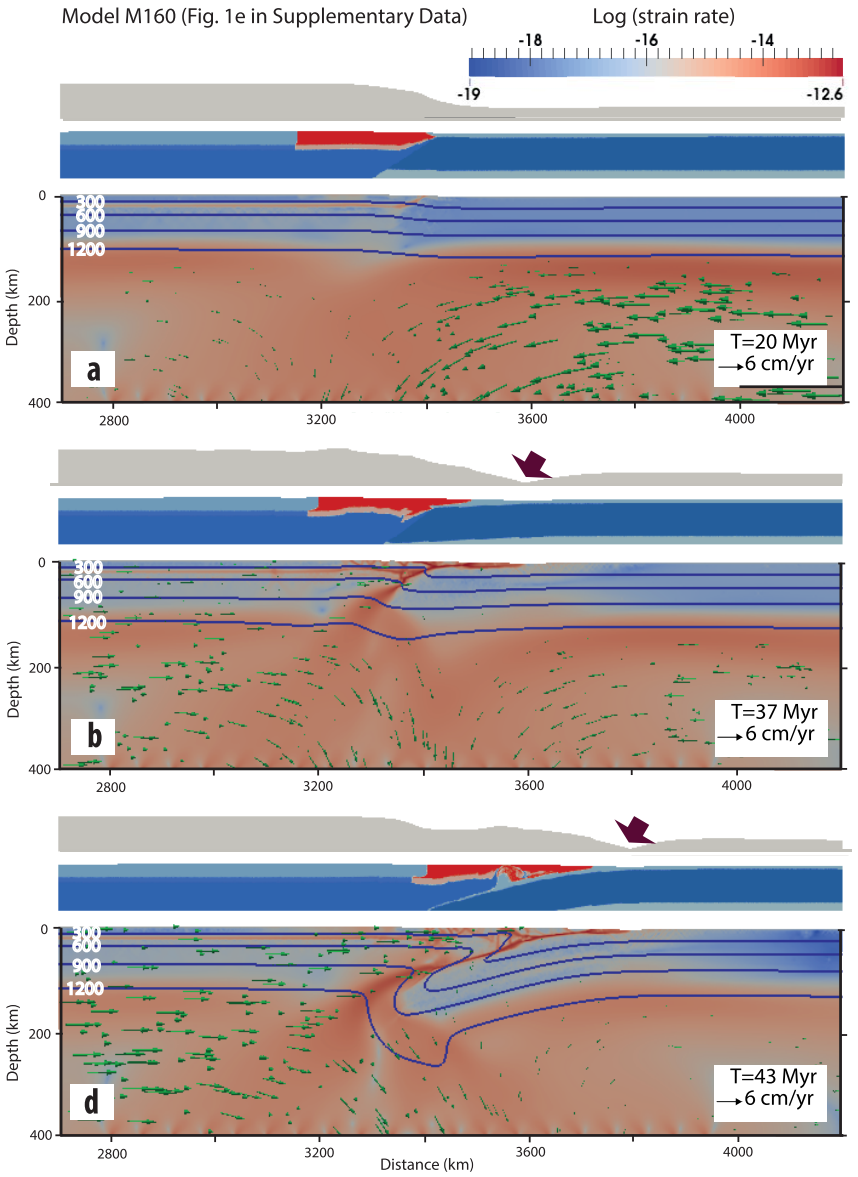

Figure 9. Model results for the evolution of the U.S. East Coast margin (see initial setup in supporting information Figure S1e). (a–c) Results of model M160 (supporting information Table S1). In this model, subduction is initiated at approximately 43 Myr. For description of the figures, see Figure 3.

the continent in this model, the shear stress induced by mantle flow is integrated over a larger distance, and generates larger compression at the passive margin than that in models for South America. As a result, even an average mantle flow velocity of 1.5 cm/yr, with a domain width of 1,200 km, centered at the passive margin (model M160 in supporting information Table S1), is sufficient to initiate subduction at approximately 43 Myr in the 2-D model setting (Figure 9). Recently, Sigloch and Mihalynuk (2017), using seismic tomography, indicated evidence of slab remnants of former subduction zones, such as the Farallon, Mezcalera, and Angayucham oceans below the North American continent. The high *P* wave velocity anomalies, which are the fragments of former subduction zones from the Early Cretaceous, are now located in upper parts of the lower mantle. This supports our scenario about sustainability of suction flow for a few tens of millions of years.

Unlike the Argentine Basin, DEM data from ETOPO5 (Noaa, http://oos.soest.hawaii.edu/erddap/griddap/etopo5.html) do not show any depressions in the surface topography along the U.S. East Coast, which is likely related to the thick sedimentary cover in this region. The DEM at latitude 33°N is in good agreement with the

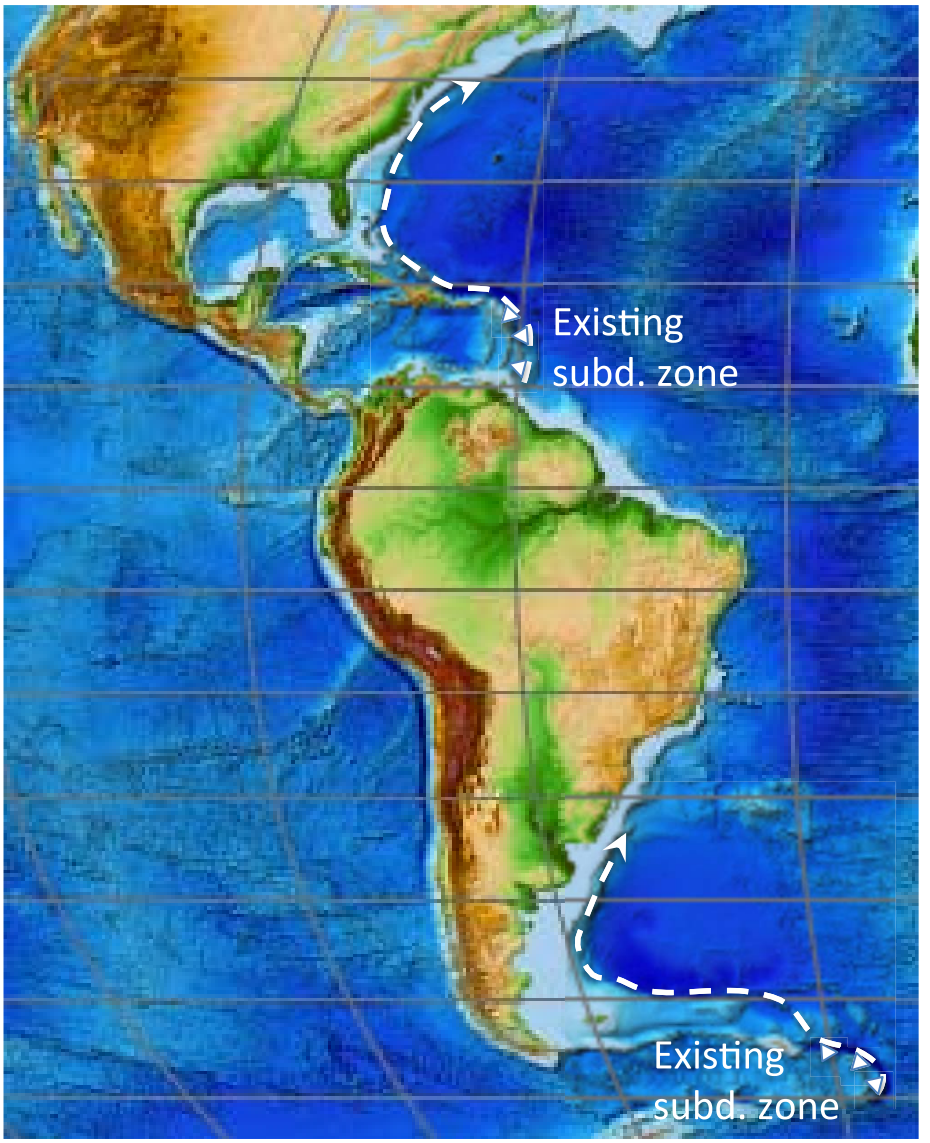

Figure 10. Possible scenarios for subduction initiation at South and North American passive margins. Subduction is initiated at the Argentinian margin, and/or the U.S. East Coast margin (see main text for details), initiation starting at the closest existing subduction zones, which are the Puerto Rico/Lesser Antilles and South Sandwich subduction zones, and propagating northward.

model results at the stage of formation of a shear zone in the upper part of the lithosphere ($t \approx 20$ Myr) (Figure 8b), indicating that conversion of the U.S. East Coast into a subduction zone may also occur in a few tens of millions of years, similar to the Argentine Basin. Note, however, that our estimates apply for the 2-D case, but in the real 3-D situation, subduction initiation may take much longer. In this respect, both the Argentine Basin and U.S. East Coast are, again, the most favorable places because they are located near already-existing subduction zones. We suggest that subduction initiation in Argentina and the U.S. East Coast will likely start from the closest existing subduction zones—Puerto Rico/Lesser Antilles and South Sandwich—and propagate along the margin, toward the north (Figure 10).

As discussed above, several conditions must be met to allow new subduction zones to form at passive margins. If mantle suction is not sufficient to break Atlantic passive margins, the margins will remain stable for hundreds of millions of years, and the Atlantic Ocean will likely grow at the expense of the closing of the Pacific Ocean, which will eventually result in collision of the Americas with Eurasia. This will increase compression at the passive margins, and may potentially trigger subduction initiation. Our numerical models, with an imposed convergence rate on the continental plate (models M157-M158 in supporting information Table S1), indicate that, even in this perhaps rather extreme scenario, the Atlantic Ocean will begin to close at some time, and the Wilson Cycle will proceed.

Relicts of past subduction zones are obviously present, not only below the continents but also below the oceans. Model results for a fracture zone in the mid-oceanic lithosphere (supporting information Table S2) show that a sufficiently strong mantle suction flow is also able to convert a fracture zone into a subduction zone, and form a new converging plate boundary in the mid-ocean. Therefore, we infer that mantle suction flow can be an efficient trigger for subduction initiation, both at continental passive margins and in the oceans. One consequence is that new subduction zones, in general, should tend to originate above the zones of former subduction. This idea may explain the remarkable colocation of subduction zones during at least the last 400 Myr (Collins, 2003; see also Figure 8).

5. Conclusions

Using 2-D numerical models, we have shown that mantle flow can act as a triggering factor for subduction initiation. Experiments exploring subduction nucleation along passive margins reveal that formation of a new subduction zone is a long-term process, explaining the lack of any Cenozoic conversion of passive margins into active ones. Subduction initiation induced by mantle flow depends on several parameters,

including the magnitude, location, and domain size of the mantle suction flow, strength of the crust near the margin, and topographic gradient within the continent. Our experiments show that mantle suction flow is able to trigger subduction initiation, both at passive margins and in mid-ocean settings. This indicates the tendency of new subduction zones to originate above zones of former subduction.

We suggest that there are at least two localities on Earth where subduction may form along passive margins as a result of induced forces from mantle suction flow. These locations are the Argentine passive margin and the U.S. East Coast, where dynamic topography indicates a considerable negative anomaly below these regions. We believe that subduction initiation is most likely in the initial stage of shear zone formation in the upper parts of the lithosphere, and self-sustained subduction may be initiated in a few tens of Myr.

Acknowledgments
The necessary data to reproduce the numerical models are available in the supporting information. Marzieh Baes was funded by a Helmholtz Postdoctoral Fellowship. We thank Javier Quinteros, Anton Popov, and Jens Tympel for helping with the design of the numerical models. We are also grateful to Elvira Mulyukova and Sasha Brune for commenting on an earlier version of the manuscript. Oğuz Göğüş and two anonymous reviewers are thanked for their constructive comments.

References

Becker, T. W., & Faccenna, C. (2011). Mantle conveyor beneath the Tethyan collisional belt. *Earth and Planetary Science Letters*, *310*, 453–461.

Becker, T. W., & O'Connell, R. J. (2001). Predicting plate velocities with mantle circulation models. *Geochemistry, Geophysics, Geosystems*, *2*(12), 1060. https://doi.org/10.1029/2001GC000171

Bijwaard, H., Spakman, W., & Engdahl, E. R. (1998). Closing the gap between regional and global travel time tomography. *Journal of Geophysical Research*, *103*, 30055–30078.

Brune, S., Heine, C., Perez-Gussinye, M., & Sobolev, S. V. (2014). Rift migration explains continental margin asymmetry and crustal hyperextension. *Nature Communications*, *5*, 4014. https://doi.org/10.1038/ncomms5014

Brune, S., Popov, A., & Sobolev, S. V. (2012). Modeling suggests that oblique extension facilitates rifting and continental break-up. *Journal of Geophysical Research*, *117*, B08402. https://doi.org/10.1029/2011JB008860

Cloetingh, S., Wortel, R., & Vlaar, N. (1982). Evolution of passive continental margins and initiation of subduction zones. *Geologica Ultraiecrina*, *29*, 1–111.

Cloetingh, S., Wortel, R., & Vlaar, N. (1984). Passive margin evolution, initiation of subduction and the Wilson cycle. *Tectonophysics*, *109*, 147–163.

Cloetingh, S., Wortel, R., & Vlaar, N. (1989). On the initiation of subduction zones. *Pure and Applied Geophysics*, *129*, 7–25.

Collins, W. (2003). Slab pull, mantle convection, and Pangaean assembly and dispersal. *Earth and Planetary Science Letters*, *205*, 225–237.

Conrad, C. P., & Lithgow-Bertelloni, C. (2007). Faster seafloor spreading and lithosphere production during the mid-Cenozoic. *Geology*, *35*, 29–32.

Duarte, J. C., Rosas, F. M., Terrinha, P., Schellart, W. P., Boutelier, D., Gutscher, M.-A., & Ribeiro, A. (2013). Are subduction zones invading the Atlantic? Evidence from the southwest Iberia margin. *Geology*, *41*, 839–842.

Faccenna, C., Giardini, D., Davy, P., & Argentieri, A. (1999). Initiation of subduction at Atlantic-type margins: Insights from laboratory experiments. *Journal of Geophysical Research*, *104*, 2749–2766.

Fei, H., Wiedenbeck, M., Yamazaki, D., & Katsura, T. (2013). Small effect of water on upper-mantle rheology based on silicon self-diffusion coefficients. *Nature*, *498*, 213–215.

Flament, N., Gurnis, M., & Müller, R. D. (2013). A review of observations and models of dynamic topography. *Lithosphere*, *5*, 189–210.

Gleason, G. C., & Tullis, J. (1995). A flow law for dislocation creep of quartz aggregates determined with the molten salt cell. *Tectonophysics*, *247*, 1–23.

Goes, S., Capitanio, F. A., & Morra, G. (2008). Evidence of lower-mantle slab penetration phases in plate motions. *Nature*, *451*, 981–984.

Gurnis, M., Hall, C., & Lavier, L. (2004). Evolving force balance during incipient subduction. *Geochemistry, Geophysics, Geosystems*, *5*, Q07001. https://doi.org/10.1029/2003GC000681

Hall, C. E., Gurnis, M., Sdrolias, M., Lavier, L. L., & Müller, R. D. (2003). Catastrophic initiation of subduction following forced convergence across fracture zones. *Earth and Planetary Science Letters*, *212*, 15–30.

Hirth, G., & Kohlstedt, D. (2003). Rheology of the upper mantle and the mantle wedge: A view from the experimentalists. In *Inside the subduction Factory* (pp. 83–105). Washington, DC: American Geophysical Union.

Karato, S. I., Paterson, M. S., & FitzGerald, J. D. (1986). Rheology of synthetic olivine aggregates: Influence of grain size and water. *Journal of Geophysical Research*, *91*, 8151–8176.

Kemp, D. V., & Stevenson, D. J. (1996). A tensile, flexural model for the initiation of subduction. *Geophysical Journal International*, *125*, 73–93.

Leng, W., & Gurnis, M. (2015). Subduction initiation at relic arcs. *Geophysical Research Letters*, *42*, 7014–7021. https://doi.org/10.1002/2015GL064985

Li, Z., Ni, S., & Somerville, P. (2014). Resolving shallow shear-wave velocity structure beneath station CBN by waveform modeling of the Mw 5.8 mineral, Virginia, earthquake sequence. *Bulletin of the Seismological Society of America*, *104*, 944–952.

Lu, G., Kaus, B. J., Zhao, L., & Zheng, T. (2015). Self-consistent subduction initiation induced by mantle flow. *Terra Nova*, *27*, 130–138.

Marques, F. O., Nikolaeva, K., Assumpção, M., Gerya, T. V., Bezerra, F. H., do Nascimento, A. F., & Ferreira, J. M. (2013). Testing the influence of far-field topographic forcing on subduction initiation at a passive margin. *Tectonophysics*, *608*, 517–524.

McKenzie, D. (1977). The initiation of trenches. In *Island arcs, deep sea trenches and back-arc basins* (pp. 57–61). Washington, DC: American Geophysical Union.

Nikolaeva, K., Gerya, T., & Marques, F. (2010). Subduction initiation at passive margins: Numerical modeling. *Journal of Geophysical Research*, *115*, B03406. https://doi.org/10.1029/2009JB006549

Popov, A., & Sobolev, S. (2008). SLIM3D: A tool for three-dimensional thermomechanical modeling of lithospheric deformation with elasto-visco-plastic rheology. *Physics of the Earth and Planetary Interiors*, *171*, 55–75.

Regenauer-Lieb, K., Yuen, D. A., & Branlund, J. (2001). The initiation of subduction: Criticality by addition of water? *Science*, *294*, 578–580.

Rybacki, E., & Dresen, G. (2000). Dislocation and diffusion creep of synthetic anorthite aggregates. *Journal of Geophysical Research*, *105*, 26017–26036.

Seton, M., Müller, R., Zahirovic, S., Gaina, C., Torsvik, T., Shephard, G., . . . Maus, S. (2012). Global continental and ocean basin reconstructions since 200Ma. *Earth Science Reviews*, *113*, 212–270.

Shephard, G., Liu, L., Müller, R., & Gurnis, M. (2012). Dynamic topography and anomalously negative residual depth of the Argentine Basin. *Gondwana Research*, *22*, 658–663.

Sigloch, K. (2011). Mantle provinces under North America from multifrequency |*P*| wave tomography. *Geochemistry, Geophysics, Geosystems*, *12*, Q02W08. https://doi.org/10.1029/2010GC003421

Sigloch, K., & Mihalynuk, M. G. (2017). Mantle and geological evidence for a Late Jurassic–Cretaceous suture spanning North America. *GSA Bulletin*, *129*, 1489–1520.

Steinberger, B. (2007). Effects of latent heat release at phase boundaries on flow in the Earth's mantle, phase boundary topography and dynamic topography at the Earth's surface. *Physics of the Earth and Planetary Interiors*, *164*, 2–20.

Stern, R. J. (2004). Subduction initiation: Spontaneous and induced. *Earth and Planetary Science Letters*, *226*, 275–292.

Toth, J., & Gurnis, M. (1998). Dynamics of subduction initiation at preexisting fault zones. *Journal of Geophysical Research*, *103*, 18053–18067.

Turcotte, D., & Schubert, G. (1982). *Geodynamics: Applications of continuum physics to geological problems* (450 pp.). New York, NY: John Wiley.

van der Lee, S., Regenauer-Lieb, K., & Yuen, D. A. (2008). The role of water in connecting past and future episodes of subduction. *Earth and Planetary Science Letters*, *273*, 15–27.

Vietor, T., & Echtler, H. (2006). Episodic Neogene southward growth of the Andean subduction Orogen between 30°S and 40°S—plate motions, mantle flow, climate, and upper-plate structure. In *The Andes* (pp. 375–400). Berlin, Germany: Springer.

Wilson, J. T. (1966). Did the Atlantic close and then re-open? *Nature*, *211*, 676–681.